eLife

Reviewed Preprint
v1 • August 5, 2026
Not revised

For correspondence:
ma.shaohua@sz.tsinghua.edu.cn

# These authors contribute equally to this work

Competing interests: No competing interests declared

Funding: See page 14

Reviewing editor: Florent Ginhoux, Singapore Immunology Network, Singapore

An integrated human forebrain organoid reveals microglia-mediated CD8$^+$ T cell recruitment and neuroimmune dysfunction in Alzheimer's disease pathology

Yilin Feng[1,#], Feifei Yu[1,#], Jiyuan Tang[1,#], Honghui Zheng[1], Zitian Wang[1,3], Shaohua Ma[1,2,3]

[1]Institute of Biopharmaceutical and Health Engineering (iBHE), Tsinghua Shenzhen International Graduate School (SIGS), Tsinghua University, Shenzhen, China • [2]Key Laboratory of Industrial Biocatalysis, Ministry of Education, Tsinghua University, Beijing, China • [3]Key Laboratory of Active Proteins and Peptides Green Biomanufacturing of Guangdong Higher Education Institutes, Tsinghua Shenzhen International Graduate School, Shenzhen, China

eLife Assessment

This study presents a **valuable** human organoid platform for investigating neuron-immune interactions in Alzheimer's disease and modeling the interplay between innate and adaptive immunity in the context of amyloid pathology. The system has the potential to advance the field by enabling the study of human-specific neuroimmune interactions that are difficult to recapitulate in rodent models; however, the evidence supporting several central conclusions remains **incomplete**. Key claims, including the causal role of microglia-derived chemokines in T cell recruitment and the existence of a neuroinflammatory feedback loop, rely primarily on correlative observations and lack the mechanistic experiments necessary to establish causality; in addition, a major confounding factor, the non-autologous nature of the cellular components, is not adequately addressed. Despite these limitations, the study will be of considerable interest to researchers in neuroimmunology and Alzheimer's disease.

https://doi.org/10.7554/eLife.111730.1.sa2

Abstract

Genetic evidence implicates immune dysfunction in Alzheimer's disease (AD), yet human-specific neuroimmune mechanisms remain poorly defined. Here, we establish a modular human forebrain organoid platform that systematically integrates iPSC-derived microglia and CD8$^+$ T cells to reconstitute multicellular Alzheimer's disease pathology. This system enables functional interrogation of both innate and adaptive immune components in a human-relevant context. Using this platform, we demonstrate that microglia mediate amyloid-β clearance and neuronal maturation but also drive inflammatory activation and recruit CD8$^+$ T cells through CCL4/5-CXCL10 signaling via CCR1/5 and CXCR3, establishing a neuroinflammatory feedback loop. Pharmacological targeting of CCR5 or CXCR3 blocks T cell recruitment and modulates autophagy in a microglia-dependent manner. This modular organoid platform provides a versatile tool for dissecting neuron–immune interactions and enables cell-type-specific therapeutic screening in human neuroinflammatory disease models.

Highlights

1. A modular human forebrain organoid platform integrating innate (microglia) and adaptive (CD8$^+$ T cells) immunity recapitulates key features of the human neuroimmune environment

2. Enables mechanistic dissection of multicellular interactions underlying Alzheimer's disease pathology
3. Overcomes limitations of traditional animal models by resolving human-specific, cell-type-specific neuroimmune mechanisms
4. Establishes a new approach methodology for studying neuroimmune disorders and advancing drug discovery

Introduction

Alzheimer's disease (AD) is featured by amyloid-beta (Aβ) accumulation, which triggers a complex cascade of glial activation, neuroinflammation, and neuronal damage (1,2). While resident microglia and astrocytes drive much of this local neuroinflammatory landscape (4,5,8,9,10), emerging evidence highlights the active infiltration of adaptive immune cells - particularly CD8+ T cells - into the AD brain parenchyma (ref). We previously demonstrated in transgenic mouse models that CD8+ T cells are enriched at pathological lesions and play an essential role in AD progression (cell reports 2023). However, the precise mechanisms governing their recruitment and their interplay with resident central nervous system (CNS) cells remain poorly understood, largely due to profound translational gaps between murine models and human immunity.

The CCL5-CCR5 chemokine signaling axis has emerged as a critical node integrating these cellular responses (13,14). Expressed on both CNS resident cells and peripheral immune cells, the CCR5 receptor and its glial-derived ligand CCL5 facilitate both local neuroinflammation and the chemotactic infiltration of CD8+ T cells (16). Yet, determining the exact, cell-type-specific roles of CCL5-CCR5 and other signaling pathways (20) in human AD has been stalled by a lack of experimental systems capable of faithfully capturing human, multicellular neuroimmune dynamics.

To bridge this fundamental gap, we engineered a modular, human forebrain organoid platform that systematically reconstructs both innate and adaptive neuroimmune microenvironments. Unlike traditional 2D cultures or in vivo murine models, this 3D system structurally and functionally integrates human induced pluripotent stem cell (iPSC)-derived forebrain organoids (21, nat commun 2025) with iPSC-derived microglia (ref) and primary peripheral CD8+ T cells. By exposing this platform to the highly amyloidogenic Aβ42 isoform, we established an experimentally tractable, tri-cellular model that dynamically mimics the human AD neuroinflammatory milieu.

Crucially, the modular nature of this platform permits precise spatiotemporal control over cellular composition, stepwise tracking of T cell infiltration, and real-time functional readouts of neuro-glial-T cell crosstalk. Utilizing this system, we successfully recapitulated key features of human AD immune dysfunction, dissected the human-specific mechanisms translating Aβ pathology into T cell recruitment, and identified and verified novel immunomodulatory cues. Ultimately, this integrated organoid platform provides a comprehensive and versatile framework for dissecting complex neuroimmune interactions and identifying cell-type-specific therapeutic targets in AD.

Result

Aβ42 Impairs Forebrain Organoid Maturation and Induces a Stress-Associated State

To establish a human neural substrate for modeling Alzheimer's disease (AD), we differentiated forebrain organoids from human iPSCs and exposed them to Aβ42 oligomers for 8 days beginning at day 90 of differentiation (Fig. 1A). Immunofluorescence staining confirmed the presence of cortical progenitor and neuronal populations, including $TBR2^+$, $CTIP2^+$, and $SOX2^+$ cells (Fig. 1B) as well as $SATB2^+$, $CTIP2^+$, and $BRN2^+$ neurons (Fig. 1C), in both control (CTR) and Aβ42-treated organoids. Forebrain regional identity was maintained following Aβ42 exposure, as evidenced by sustained expression of FOXG1, MAP2, SOX2, and PAX6 (Fig. 1D). Astrocyte-associated

populations expressing GFAP and S100B were also present in both conditions (Fig. 1E). Immunostaining with the 6E10 antibody confirmed significant Aβ accumulation in treated organoids (Fig. 1F; $P < 0.0001$).

To characterize the transcriptional impact of Aβ42 exposure, we performed single-cell RNA sequencing on day 90 CTR and Aβ42-treated organoids. UMAP visualization of integrated data revealed diverse neural cell types, including radial glia, intermediate progenitor cells (IPCs), migrating neurons, maturing neurons, and upper-layer excitatory neurons (Fig. 1G). Comparison of relative cell-type proportions showed shifts following Aβ42 treatment, including an increase in stress-responsive populations and a decrease in maturing neurons (Fig. 1H). Pseudobulk differential expression analysis revealed upregulation of stress-associated genes and downregulation of neuronal maturation-related genes in Aβ42-treated organoids (Fig. 1I). Gene set enrichment analysis (GSEA) confirmed activation of cellular stress pathways and depletion of neuronal maturation programs (Fig. 1J). Pseudotime trajectory analysis using Monocle3 showed that Aβ42-treated organoids exhibited a significant shift toward lower pseudotime values compared with CTR (Fig. 1K-L; Wilcoxon rank-sum test), indicating that Aβ42 exposure arrests cells in an immature, stress-associated state.

Together, these data establish that Aβ42 exposure alone induces transcriptional stress and impairs neuronal maturation in human forebrain organoids, creating a vulnerable neural substrate for subsequent immune interactions.

A 2D-3D Hybrid Organoid System Enables Functional Interrogation of Aβ42-Induced Synaptic and Network Dysfunction

To enable functional analysis of Aβ42-induced pathology, we developed a 2D-3D hybrid organoid system. Day 90 cortical organoids were either maintained as intact 3D structures for bulk RNA-seq analysis or sectioned into 300-μm slices and cultured on Matrigel-coated plates, preserving three-dimensional cytoarchitecture while providing optical access for imaging (Fig. 2B). Bulk RNA-seq of intact 3D organoids confirmed that Aβ42 treatment induced transcriptional changes consistent with our single-cell data, including upregulation of stress-associated genes and downregulation of maturation-related genes (Fig. 2A).

We next used the hybrid system to assess synaptic and network-level consequences of Aβ42 exposure. Immunofluorescence staining for synaptic markers revealed a significant shift in excitatory/inhibitory balance: Aβ42-treated organoids exhibited increased density of $VGLUT^+$ excitatory synapses and decreased density of $GABA^+$ inhibitory synapses, normalized to synaptophysin (Fig. 2C-G). This synaptic imbalance was accompanied by functional network alterations. Calcium imaging revealed significantly increased spike frequency per cell in Aβ42-treated hybrid organoids compared with CTR (Fig. 2H-I). Furthermore, GABA response analysis showed an altered post-/pre-treatment spike count ratio in Aβ42-treated organoids (Fig. 2J), suggesting impaired inhibitory signaling.

These results demonstrate that Aβ42 exposure induces both synaptic imbalance and network hyperactivity in human forebrain organoids, establishing functional deficits that recapitulate key features of AD pathophysiology.

Integration of iPSC-Derived Microglia Modulates Aβ42-Associated Transcriptional States and Neural Activity

Having established a Aβ42-exposed neural substrate with defined functional deficits, we next sought to incorporate innate immunity. We generated iPSC-derived microglia (iMGLs) through sequential differentiation of hematopoietic progenitors to immature and then mature microglia (Fig. 3A). Flow cytometry confirmed that approximately 96% of cells were $CD11b^+$, with ~50% exhibiting a $CD45^{low}$ phenotype consistent with microglial maturation (Fig. 3B). When co-cultured with Aβ42-treated organoids, iMGLs associated with and engulfed Aβ42 oligomers, as

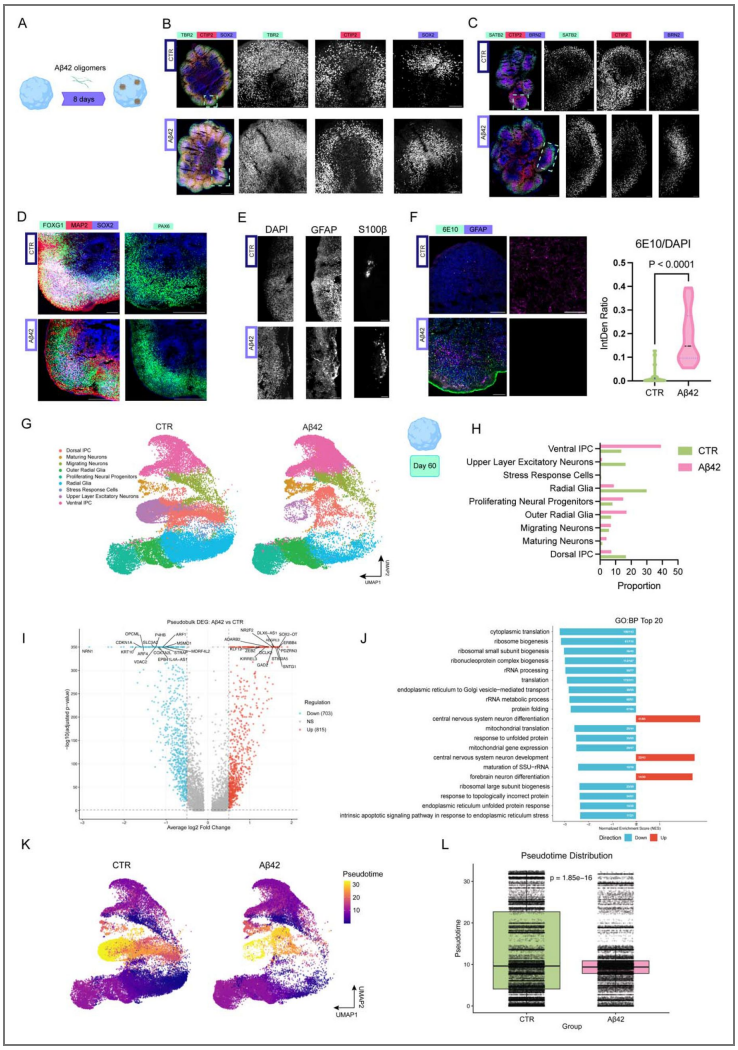

Figure 1. Aβ impairs forebrain organoid maturation and induces stress-associated states.

(A) Schematic of the experimental design. Forebrain organoids were differentiated and exposed to Aβ42 oligomers for 8 days starting at day 90. (B–C) Immunofluorescence staining of cortical progenitor and neuronal layer markers in control (CTR) and Aβ42-treated organoids. Expression of TBR2, CTIP2, and SOX2 (B), and SATB2, CTIP2, and BRN2 (C), confirms the presence of cortical progenitor and neuronal populations in both CTR and Aβ42-treated organoids. The section sizes do not represent organoid size difference. (D) Representative immunofluorescence images showing expression of forebrain markers FOXG1, MAP2, SOX2, and PAX6 in CTR and Aβ42-treated organoids, indicating maintenance of forebrain regional identity following Aβ42 exposure. (E) Immunostaining for glial markers GFAP and S100B in CTR and Aβ42-treated organoids, demonstrating the presence of astrocyte-associated populations in both conditions. (F) Detection of Aβ using the 6E10 antibody in CTR and Aβ42-treated organoids. Quantification of 6E10 signal intensity normalized to DAPI shows significantly increased Aβ signal in treated organoids (right; violin plot, P < 0.0001, unpaired t test, n = 4–6 organoids per group). (G) UMAP visualization of integrated single-cell RNA-seq data from day 60 CTR and Aβ42-treated organoids, split by condition and colored by annotated cell types. (H) Comparison of relative cell-type proportions between CTR and Aβ42-treated organoids reveals shifts in the abundance of specific transcriptional states following Aβ treatment. (I) Volcano plot showing differentially expressed genes identified by pseudobulk analysis comparing Aβ42-treated organoids to CTR, highlighting induction of stress-associated genes and reduced expression of neuronal maturation–related genes. (J) Gene set enrichment analysis (GSEA) performed on Gene Ontology Biological Process (GO:BP) terms using differentially expressed genes from pseudobulk analysis comparing Aβ42-treated organoids to CTR. Enriched pathways highlight activation of cellular stress–related processes and depletion of neuronal maturation–associated biological processes in Aβ42-treated organoids. (K) Pseudotime trajectory analysis inferred using Monocle3 and visualized on UMAP embeddings for control (CTR; left) and Aβ42-treated (right) organoids, showing differences in the distribution of cells along the inferred neurogenic trajectory between conditions. (L) Quantification of pseudotime distributions in CTR and Aβ42-treated organoids. Aβ42-treated organoids exhibit a significant shift toward lower pseudotime values compared with CTR (Wilcoxon rank-sum test).

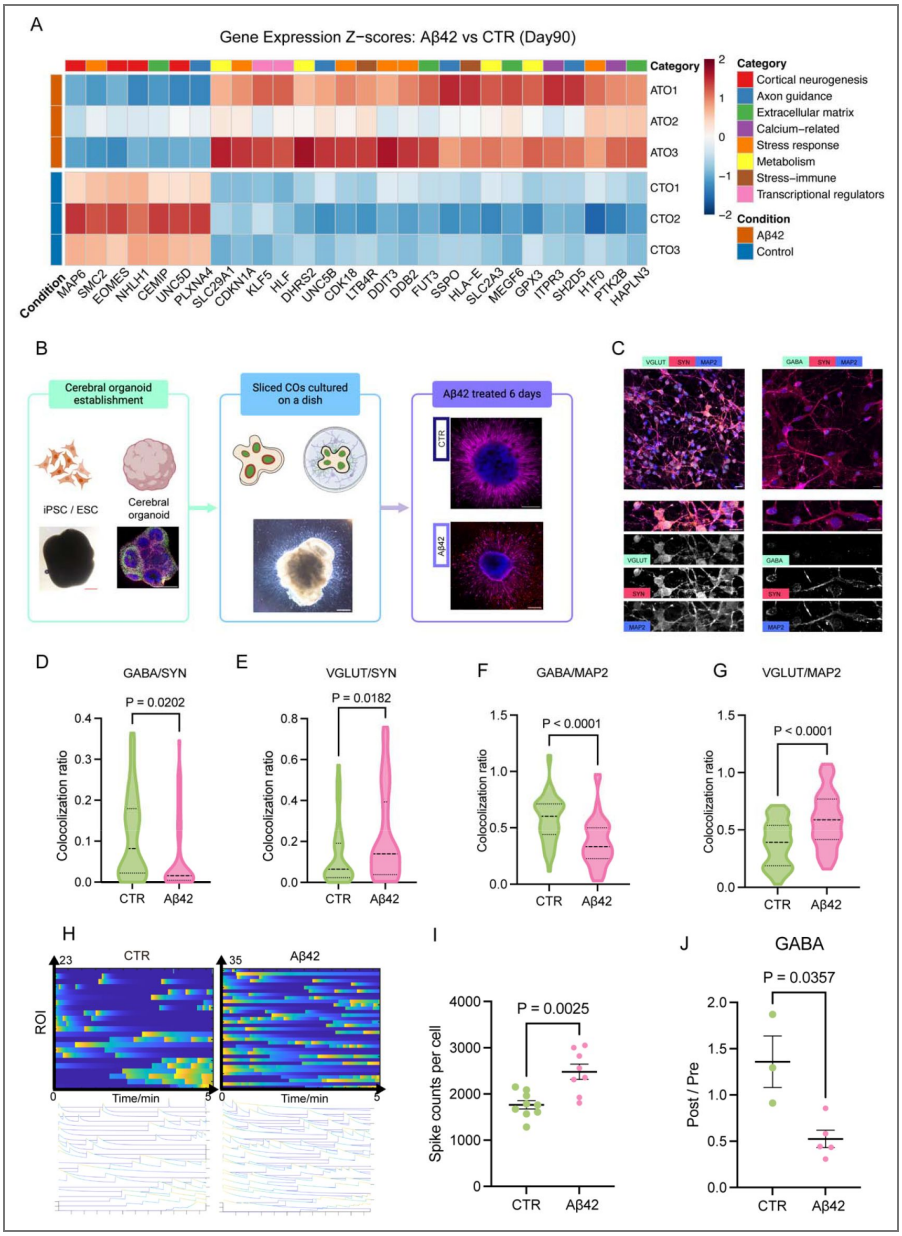

Figure 2. Development and characterization of a 2D–3D hybrid organoid model for analyzing Aβ42-induced pathology.

(A) Heatmap of the top 30 most significantly differentially expressed genes from bulk RNA-seq analysis of day 90 3D Aβ42-treated and CTR organoids. Expression values are shown as scaled normalized expression across individual samples, with hierarchical clustering applied to both genes and samples. (B) Experimental workflow for the study. Day 90 cortical organoids were either maintained as intact 3D organoids for bulk RNA-seq analysis or sectioned into 300-μm slices and cultured on Matrigel-coated plates to generate a 2D–3D hybrid organoid system for synaptic and functional analyses. Hybrid cultures were treated with 5 μM Aβ42 oligomers for 6 days prior to downstream assays. (C) Representative immunofluorescence images of co-stained Syn, MAP2 with VGLUT or GABA to assess synapse ratio. Scale bar: 10 μm. (D–G) Quantitative analysis of synaptic marker density in CTR and Aβ42-treated 2D–3D hybrid organoids. Measurements of excitatory synapses (VGLUT/synaptophysin) and inhibitory synapses (GABA/synaptophysin) reveal increased excitatory and decreased inhibitory synaptic density in Aβ42-treated organoids. (H) Representative calcium imaging traces recorded from CTR and Aβ42-treated 2D–3D hybrid organoids. Images were acquired at 7.67 s per frame. (I) Quantification of calcium imaging data showing increased spike frequency per cell in Aβ42-treated hybrid organoids compared with CTR. (J) GABA response analysis expressed as the post-/pre-treatment spike count ratio, indicating altered GABA responsiveness in Aβ42-treated hybrid organoids. Data are presented as mean ± SEM. For immunofluorescence and functional analyses, n = 4–6 organoids per group. Statistical significance was assessed using unpaired t tests.

visualized by IBA1 and 6E10 co-staining (Fig. 3B). ELISA quantification of culture media showed that iMGL integration significantly reduced Aβ42 levels compared with organoids alone (Fig. 3C; $P < 0.0001$), confirming functional Aβ clearance.

To understand how microglia reshape the cellular landscape, we performed single-cell RNA sequencing on Aβ42-treated organoids with and without iMGL co-culture (Aβ42+iMGL and Aβ42 conditions). UMAP visualization revealed the appearance of a distinct microglial cluster in the Aβ42+iMGL group, with all major neural populations preserved (Fig. 3D). Comparison of cell-type proportions showed shifts following microglial integration, including changes in progenitor and neuronal subtypes (Fig. 3E). Strikingly, pseudotime analysis revealed that microglial co-culture significantly shifted cells toward higher pseudotime values compared with Aβ42 alone (Fig. 3F-G; P = 2.17e-16), indicating that microglia promote neuronal maturation and partially reverse the Aβ42-induced immature state.

Cell-cell interaction analysis using CellChat identified extensive signaling networks between microglia and neural populations (Fig. 3H). Microglia exhibited both outgoing signals, including neurotrophic (PTN, IGF1), synaptic (NRXN3-NLGN1), and immunomodulatory (LGALS9-HAVCR2) pathways, and incoming signals from neural progenitors and neurons (Fig. 3I-J), revealing bidirectional communication.

We next assessed the functional impact of microglial integration using the 2D-3D hybrid system (Fig. 3K). Calcium imaging with Fluo-4-labeled neurons and CellTracker CMTPX-labeled microglia (Fig. 3L) revealed that, in the presence of microglia, the Aβ42-induced neuronal hyperactivity was normalized: there was no significant difference in spike frequency between CTR+iMGL and Aβ42+iMGL conditions (Fig. 3M). However, microglia themselves exhibited significantly increased calcium activity in the Aβ42+iMGL condition compared with CTR+iMGL (Fig. 3N; P = 0.0346), indicating that while microglia protect neurons from hyperactivity, they become activated in the Aβ environment.

These data demonstrate that microglia integrate into forebrain organoids, clear Aβ, promote neuronal maturation, and normalize network activity, yet simultaneously enter a hyperactive state, revealing their dual functionality in AD pathology.

Microglia Drive CD8$^+$ T Cell Recruitment and Establish a Pathological Neuroimmune Tri-Cellular Unit

The persistent hyperactive state of microglia in Aβ42 environments prompted us to examine their inflammatory output. Conditioned media from CTR+iMGL and Aβ42+iMGL organoids were analyzed for cytokine and chemokine secretion. Aβ42+iMGL organoids exhibited significantly elevated levels of CCL4, CCL5, IL-1β, and TGF-β1, with no change in CXCL10 (Fig. 4A-E). These chemokines are known chemoattractants for adaptive immune cells, particularly CD8$^+$ T cells.

To test whether microglial-derived signals recruit CD8$^+$ T cells, we established a transwell migration assay using the 2D-3D hybrid system (Fig. 4F). In the absence of microglia, CD8$^+$ T cells showed no significant migration toward either CTR or Aβ42-treated organoids (Fig. 4G). However, when microglia were present, Aβ42-treated organoids induced significantly increased T cell migration compared with CTR+iMGL (Fig. 4G). This recruitment was mediated by chemokine receptors on T cells: pharmacological inhibition of CCR5, CXCR3, or CCR1 significantly reduced migration toward Aβ42+iMGL organoids (Fig. 4H).

We next established a tri-culture system to visualize and quantify microglia-T cell interactions (Fig. 4I). Forebrain organoids were treated with Aβ42 for 6 days, co-cultured with iMGLs for 48 hours, and then CD8$^+$ T cells were added 24 hours prior to calcium imaging. Multi-channel imaging enabled simultaneous visualization of T cells (CellTrace Violet), calcium activity (Fluo-4 AM), microglia (CellTracker CMTPX), and Aβ42 (647 nm) (Fig. 4J). Time-lapse imaging revealed heterogeneous microglial activation states, with some microglia engaging in direct T cell interactions and others exhibiting Aβ42-associated activity (Fig. 4K).

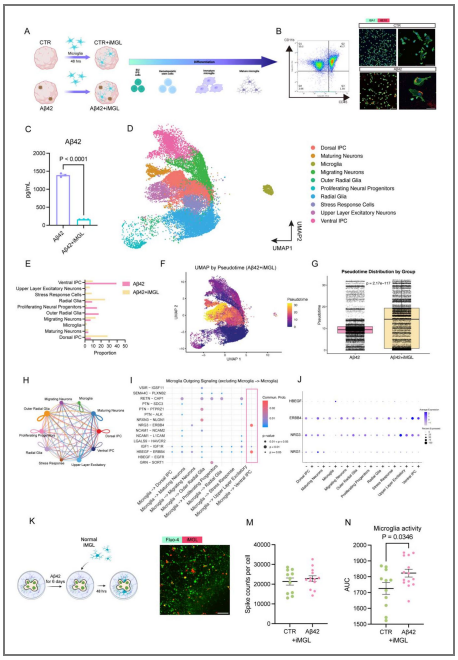

Figure 3. Integration of iPSC-derived microglia modulates Aβ42-associated transcriptional states and neural activity in forebrain organoids.

(A) Experimental scheme illustrating the microglia-integrated forebrain organoid model. Forebrain organoids were treated with vehicle (0.1% DMSO; CTR) or Aβ42 oligomers (5 μM) for 6 days, followed by a 48-hour co-culture with iPSC-derived microglia (iMGLs) to generate CTR+iMGL and Aβ42+iMGL conditions. The workflow depicts iPSC differentiation through hematopoietic progenitors, immature microglia, and mature microglia stages. (B) Characterization of iPSC-derived microglia. Flow cytometry analysis (left) shows that approximately 96% of cells are CD11b+ and ~50% exhibit a CD45^low phenotype, consistent with microglial maturation. Representative immunofluorescence images (right) show iMGLs labeled with IBA1 (green) and Aβ42 detected by 6E10 (red), demonstrating association and engulfment of Aβ42 oligomers by iMGLs. Scale bars: 100 μm (overview), 50 μm (high magnification). (C) Quantification of Aβ42 levels in culture medium by ELISA 48 hours after iMGL integration. Aβ42 levels are significantly reduced in the Aβ42+iMGL condition compared with Aβ42-treated forebrain organoids without microglia ($P < 0.0001$, unpaired t test, n = 3 samples per group). Data are presented as mean ± SEM. (D) UMAP visualization of integrated single-cell RNA-seq data from Aβ42-treated forebrain organoids (Aβ42) and Aβ42-treated forebrain organoids co-cultured with microglia (Aβ42+iMGL), split by condition and colored by annotated cell types. Major neural progenitor and neuronal populations are present in both conditions, with the appearance of a microglial cluster (yellow) in the Aβ42+iMGL group. (E) Comparison of relative cell-type proportions between Aβ42-treated forebrain organoids with (Aβ42+iMGL) and without (Aβ42) microglial co-culture, revealing shifts in the abundance of specific transcriptional states following microglial integration. (F) Pseudotime trajectory analysis inferred using Monocle3 and visualized on UMAP embeddings for Aβ42+iMGL condition, showing the distribution of cells along inferred developmental trajectories. Colors represent pseudotime values from early (purple/blue) to late (yellow/red) developmental states. (G) Quantification of pseudotime distributions comparing Aβ42-treated forebrain organoids with and without microglial co-culture. Aβ42+iMGL organoids exhibit a significant shift toward higher pseudotime values compared with Aβ42 alone ($p = 2.17e\text{-}16$, Wilcoxon rank-sum test). Box plots show median, quartiles, and individual data points. (H) Cell-cell interaction network analysis showing predicted signaling pathways between cell types in Aβ42+iMGL organoids. Node size and edge thickness represent interaction strength. Colors indicate different cell populations including microglia, various neuronal subtypes, and progenitor cells. (I, J) Microglia outgoing (I) and incoming (J) signaling with environmental cells for various signaling pathways. (K) Experimental design for functional analyses using the 2D–3D hybrid forebrain organoid system.Organoid slices were treated with Aβ42 (5 μM) for 6 days, followed by a 48-hour co-culture with iPSC-derived microglia prior to calcium imaging. (L) Representative calcium imaging field showing neuronal calcium activity labeled with Fluo-4 (green) and iPSC-derived microglia labeled with CellTracker CMTPX (red) in Aβ42-treated hybrid organoids. Scale bar: 100 μm. (M) Quantification of neuronal calcium activity (spike counts per cell) showing no significant difference between CTR+iMGL and Aβ42+iMGL conditions in the presence of microglial co-culture. Individual dots represent single cells; horizontal lines indicate mean ± SEM (n = 3–4 organoids per group). (N) Quantification of microglial calcium activity expressed as the area under the curve (AUC) of $\Delta F/F_0$ traces, showing significantly increased microglial calcium activity in Aβ42+iMGL conditions compared with CTR+iMGL ($P = 0.0346$, unpaired t test). Individual dots represent single microglia; horizontal lines indicate mean ± SEM (n = 3–4 organoids per group). 3K is created in BioRender (*https://BioRender.com/6o4kfkx*).

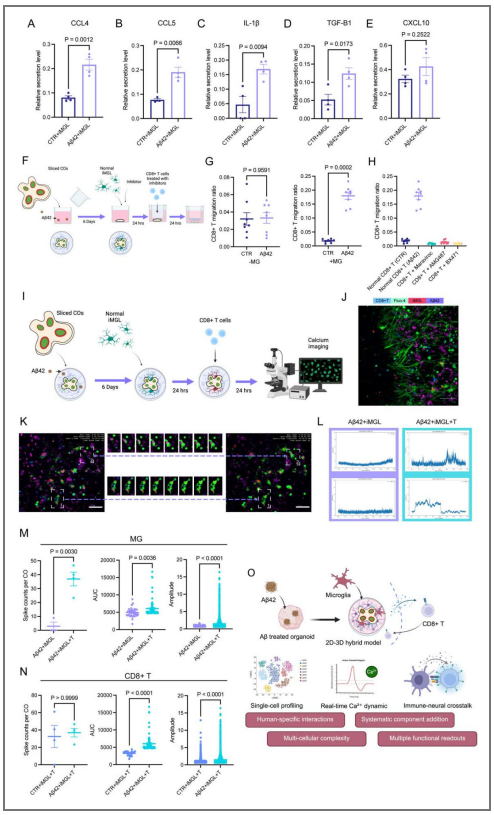

Figure 4. Aβ42-treated forebrain organoids with microglial integration promote inflammatory signaling, CD8$^+$ T cell recruitment, and microglia–T cell functional interactions.

(A–E) Quantification of inflammatory cytokine and chemokine secretion from forebrain organoids co-cultured with microglia. Relative secretion levels of CCL4 (A), CCL5 (B), IL-1β (C), TGF-β1 (D), and CXCL10 (E) were measured in conditioned media from CTR+iMGL and Aβ42+iMGL groups. Data are presented as mean ± SEM. Statistical significance was assessed using unpaired t tests. (F) Experimental schematic of the 2D–3D hybrid forebrain organoid model used to assess CD8$^+$ T cell migration. Forebrain organoids were treated with Aβ42 for 6 days and co-cultured with iPSC-derived microglia (iMGLs), followed by transwell-based migration assays using CD8$^+$ T cells with or without chemokine receptor inhibitors targeting CCR5, CXCR3, and CCR1. (G) Quantification of CD8$^+$ T cell migration in the absence (−MG) or presence (+MG) of microglial co-culture. No significant difference in migration was observed between CTR and Aβ42 conditions without microglia, whereas Aβ42-treated forebrain organoids with iMGLs exhibited significantly increased CD8$^+$ T cell migration. (H) Effects of chemokine receptor inhibition on CD8$^+$ T cell migration toward Aβ42+iMGL forebrain organoids. Blockade of CCR5, CXCR3, or CCR1 on CD8$^+$ T cells reduced migration compared with the untreated Aβ42+iMGL condition. (I) Experimental design for calcium imaging analysis of microglia–T cell interactions. iMGLs were integrated into Aβ42-treated forebrain organoids on day 6, followed by addition of CD8$^+$ T cells on day 7, with calcium imaging performed on day 8. (J) Representative multi-channel imaging showing CD8$^+$ T cells (CellTrace Violet, blue), intracellular calcium signals (Fluo-4 AM, green), iMGLs (CellTracker CMTPX, magenta), and Aβ42 (647 nm). Scale bar: 50 μm. (K) Time-lapse calcium imaging illustrating heterogeneous microglial activation states in the presence of CD8$^+$ T cells. Example regions show iMGLs engaging in direct T cell interactions or Aβ42-associated activity over a 13-minute imaging window. Scale bar: 50 μm. (L) Quantitative analysis of microglial calcium activity comparing Aβ42+iMGL and Aβ42+iMGL+T conditions. Metrics include spike count per cell, area under the curve (AUC), and spike amplitude. Individual dots represent single iMGLs. (M) Quantitative comparison of microglial calcium activity between CTR+iMGL+T and Aβ42+iMGL+T conditions using the same metrics as in (L). (N) Quantitative analysis of CD8$^+$ T cell calcium activity comparing CTR+iMGL+T and Aβ42+iMGL+Tconditions, including spike count per cell, AUC, and spike amplitude. Calcium imaging data were acquired at 3.8-s intervals. (O) Schematic overview of the integrated human forebrain organoid platform. Aβ42-treated forebrain organoids are converted to a 2D–3D hybrid system enabling systematic integration of iPSC-derived microglia and CD8$^+$ T cells. The platform supports multi-modal analysis including single-cell transcriptional profiling, real-time calcium imaging, and assessment of immune-neural cellular interactions. Key features include human-specific cellular components, multi-cellular complexity, systematic component addition, and multiple functional readouts. Data are presented as mean ± SEM. Statistical significance was assessed using unpaired t tests. For cytokine analyses, n = 3 samples per group. For migration and calcium imaging analyses, n = 3–4 organoids per group, with individual dots representing single cells where indicated. 4O is created in BioRender (*https://BioRender.com/wgpmokj*).

Quantitative analysis showed that the presence of T cells further amplified microglial hyperactivity: Aβ42+iMGL+T organoids exhibited significantly increased microglial spike count, area under the curve (AUC), and spike amplitude compared with Aβ42+iMGL without T cells (Figs. 4L, 4M). Microglial activity was also significantly higher in Aβ42+iMGL+T compared with CTR+iMGL+T (Fig. 4N), confirming that the Aβ environment drives sustained microglial activation even in the presence of T cells. $CD8^+$ T cells themselves exhibited calcium activity that was modulated by the environment, with trends toward increased activity in the Aβ42 condition (Fig. 4N).

Together, these data establish a tri-cellular neuroimmune unit in which: (1) Aβ42 creates a stressed neural substrate, (2) microglia respond by clearing Aβ and promoting maturation but become hyperactive and secrete inflammatory chemokines, (3) these chemokines recruit $CD8^+$ T cells via CCR5/CXCR3 signaling, and (4) recruited T cells further amplify microglial activation, creating a positive feedback loop of neuroinflammation (summarized in Fig. 4O).

This modular human forebrain organoid platform, incorporating both innate and adaptive immunity, enables systematic dissection of multicellular neuroimmune interactions in AD and provides an experimentally tractable system for identifying cell-type-specific therapeutic targets.

Discussion

The neuroimmune axis is central to Alzheimer's disease (AD) pathogenesis, yet the human-specific mechanisms translating amyloid pathology into sustained neuroinflammation remain poorly understood. By establishing a modular human forebrain organoid platform that sequentially integrates innate and adaptive immunity, we successfully deconstructed the tri-cellular interactions underlying AD neuroinflammation. This stepwise approach revealed a multi-stage positive feedback loop: (i) Aβ42 exposure induces neuronal stress; (ii) microglia clear Aβ (Fig. 3B-C) and normalize neuronal hyperactivity (Fig. 3M) but enter a chronically active, chemokine-secreting state (Fig. 3N, 4A-E); (iii) these microglial signals recruit $CD8^+$ T cells via CCR5/CXCR3 pathways (Fig. 4H); and (iv) the recruited T cells subsequently amplify microglial hyperactivity (Fig. 4L). Crucially, T cells failed to migrate to Aβ-treated organoids in the absence of microglia (Fig. 4G). This provides the first human-specific mechanistic demonstration that microglial activation serves as the essential bridge between amyloid pathology and the adaptive immune recruitment recently documented in human AD brains.

Furthermore, our findings experimentally resolve the functional duality of microglia in AD. Within our platform, microglia simultaneously executed protective functions—engulfing Aβ and promoting neuronal maturation (Fig. 3F-G)—while initiating pathological inflammatory cascades. This duality indicates that microglial activation is not a binary state but a spectrum, where sustained Aβ stress drives the transition from a protective to a pathological, T-cell-recruiting state. We identified the CCL5-CCR5 axis as the master integrator of this neuroimmune transition. Microglia-derived CCL5 directly drives $CD8^+$ T cell chemotaxis, while cell-cell interaction analyses revealed extensive CCR5-associated signaling with neurons and progenitors (Fig. 3H-J). Inhibiting CCR5 successfully blocked T cell recruitment (Fig. 4H) but also impacted cell-specific autophagy, indicating that CCR5 acts as a pleiotropic regulator of neuroimmune function rather than a simple chemoattractant. Repurposing clinical CCR5 antagonists (e.g., Maraviroc) or CXCR3 inhibitors offers an immediate therapeutic avenue to interrupt this pathological cascade; however, our data caution that precise modulation is necessary to suppress inflammatory outputs without sacrificing the protective clearance and maturation functions of microglia. While our 2D-3D hybrid platform captures human-specific cellular features, transcriptomic signatures, and real-time multicellular interactions unmatched by rodent or conventional in vitro models, we acknowledge several limitations. The current system lacks vasculature and additional peripheral immune populations, utilizes a single iPSC line, and reflects an acute timeline rather than decades-long disease progression. Future iterations incorporating multi-donor genetic variability - particularly AD risk variants - and extended culture periods will be critical to fully modeling disease evolution.

The modular, tri-cellular platform described here has implications beyond AD. The same approach could be applied to model other neurodegenerative and neuroinflammatory conditions, including Parkinson's disease, amyotrophic lateral sclerosis, multiple sclerosis, and neuropsychiatric disorders with immune components. By enabling systematic addition of specific immune populations - for example, different T cell subsets, B cells, or peripheral monocytes - this platform can be adapted to address diverse questions about neuroimmune interactions in health and disease.

From a therapeutic perspective, our findings identify multiple intervention points. CCR5 and CXCR3 antagonists, already in clinical use or development for other indications, could be tested for their ability to block T cell infiltration and interrupt the neuroinflammatory feedback loop. Strategies to preserve microglial protective functions (Aβ clearance, neuronal maturation) while suppressing their pathological outputs (chemokine secretion, T cell recruitment) represent a particularly attractive therapeutic goal. The platform's compatibility with high-content imaging and multi-well formats positions it for medium-throughput drug screening, and its human relevance may improve translation compared with traditional animal models.

Despite these constraints, the identification of a tri-cellular positive feedback loop offers a mechanistic explanation for the persistence of neuroinflammation in AD, even after initial pathological triggers may have subsided. Beyond AD, this modular, high-content-compatible platform provides a versatile framework to systematically dissect neuroimmune complexity, enabling the stepwise addition of distinct immune subsets to accelerate targeted drug discovery across a broad spectrum of neurodegenerative and neuropsychiatric disorders.

Methods

Animals

Male 5×FAD transgenic mice (Tg6799 line) expressing five familial AD mutations (APP K670N/M671L + I716V + V717I and PS1 M146L + L286V) and age-matched wild-type littermates were used at 8 months of age and bought from GUANGZHOU JINWEI BIOSCIENCE. Animals were housed under controlled conditions (22°C, 12-hour light/dark cycle) with ad libitum access to standard laboratory chow and water. All experimental procedures were performed in compliance with protocols approved by the Animal Experimentation Ethics Committee at Tsinghua Shenzhen International Graduate School.

Cerebral organoids, cell lines, medium and reagent

The protocol for the establishment of cerebral organoids was adapted from methods described in our previous work[21]. The cell lines used in this study included the H9 line, obtained from WiCell (Catalog # WA09), the iPSC cell line DYR0100, acquired from the National Collection of Authenticated Cell Cultures (Catalog # SCSP-1301) and DXR0109B, acquired from ATCC (Catalog #ACS-1023). Material transfer agreements (MTAs) for both the H9 and iPSC cell lines have been duly executed. The media and reagents employed for culturing these cell lines and for cerebral organoid development are detailed in our prior work.

iPSC-derived microglia

Both induced and embryonic microglia were generated following a two-step induction process. First, hematopoietic cells were derived using the STEMdiff™ Hematopoietic Kit (STEMCELL Technologies, Catalog # 05310_C). These cells were then differentiated into microglia using the STEMdiff™ Microglia Differentiation Kit (Catalog # 100-0019) and matured using the STEMdiff™ Microglia Maturation Kit (Catalog # 100-0020_C). All procedures were performed in strict accordance with the manufacturer's protocols to ensure proper induction and maturation of microglia.

2D/3D neural-immune model establishment in Aβ42 context

Cerebral organoids aged 90 days were sliced into 300 μm sections using a vibratome, following the methodology described in our previous work. The sliced COs were then cultured on 1% Matrigel-coated 12-well confocal plates, with one slice per well, to facilitate immunofluorescence imaging. Within 24 hours of culturing, neurons and astrocytes migrated outwards from the center of the COs. The culture was supplemented with 5 μM

β-amyloid (1-42) (MedChemExpress, Catalog # HY-P1363), and the medium was changed every two days. After 5 days, 1×105 induced microglia (iMGLs) were added to each well to establish the neural immune model. The samples were fixed for further analysis 48 hours after the introduction of iMGLs.

Isolation of human PBMC and CD8+ T cells

Blood specimens were collected from healthy donors at Zhangzhou People's Hospital. Peripheral blood was collected from individuals over 18 years of age in 10-ml tubes containing 5 mM EDTA. The samples were transported on ice and processed within 1-3 hours of collection. PBMCs were isolated using density gradient centrifugation with Lymphoprep™ density gradient medium (1.077 g/mL). The PBMCs were then handled with care to maintain their viability and integrity.

The human CD8+ T cells were isolated from the PBMCs using the EasySep™ Direct Human CD8+ T Cell Isolation Kit (STEMCELL Technologies, Catalog # 19663) following the manufacturer's protocols to ensure efficient and consistent isolation of CD8+ T cells.

Flow cytometry

Validation of isolated and migrated CD8+ T cells was conducted using APC/Cyanine7 anti-human CD8 Antibody (Biolegend, Catalog # 344714). For the verification of mature microglia, FITC anti-human CD45 Antibody (Biolegend, Catalog # 304006) and PE anti-human CD11b Antibody (Biolegend, Catalog # 301306) were utilized. The compensation matrix was established and positive peak gates were set based on the respective isotype controls. The isotype controls used were APC/Cyanine7 Mouse IgG1, κ Isotype Ctrl Antibody, Catalog # 400127; PE Mouse IgG1, κ Isotype Ctrl Antibody, Catalog # 400111; FITC Mouse IgG1, κ Isotype Ctrl Antibody, Catalog # 400107.

The cells were incubated with the specified antibodies for 40 minutes on ice to ensure adequate labeling. Before analysis, the cells underwent filtration through a 300-mesh Falcon centrifuge tube to eliminate aggregates and ensure a single-cell suspension. All flow cytometry data were then analyzed using FlowJo™ Software v10.10. for detailed phenotypic characterization.

Cell Tracker staining

Before conducting calcium imaging, Cell Tracker dyes were used to stain CD8+ T cells and iMGLs for better identification. CD8+ T cells were stained with CellTrace™ Violet (dilution 1:1000, Invitrogen, Catalog # C34557), and iMGLs were labeled with CellTracker™ CMTPX (dilution 1:1000, Invitrogen, Catalog # C34552). The cells were then incubated in the staining solution at 37 °C for 30 minutes. After incubation, the staining solution was removed, and the cells were cultured for future use within the next week.

Human inflammatory cytokine array

For each experimental group, 8 ml of medium was collected and concentrated using Ultrafiltration Centrifugal Tubes (Millipore, Catalog # UFC903096). The medium was reduced to a volume of 200 μl through ultrafiltration. This concentrated sample was then used to perform the Cytokine Array analysis using the Human Cytokine Antibody Array (Membrane, 42 Targets) kit (Abcam, Catalog # ab133997), strictly following the manufacturer's protocols.

Raw images of the cytokine arrays have been made available in the source data, which can be accessed via the provided Github link: *https://github.com/FengYilinElaine/2-3D-AD-oranoids*.

Immunohistochemistry

Validation of COs was based on previous work. The primary antibodies used in this study are listed in Extended Table 1.

Quantitative analysis of Aβ42 levels

Quantitative analysis of Aβ42 levels was performed using the Amyloid beta 42 Human ELISA Kit (Invitrogen, Catalog # KHB3441).

Bulk RNA sequencing analysis

Bulk RNA sequencing analysis was performed on 3D cerebral organoids, iMGLs and eMGLs, as described in the results section. The samples were collected quickly and flash-frozen in liquid nitrogen to preserve the RNA integrity. After freezing, the samples were transported on dry ice to BGI for RNA extraction and sequencing. All RNA analyses, including data processing and interpretation, were conducted on the Dr. Tom platform (BGI).

Single-cell RNA-seq Library Preparation and Sequencing

For isolation of iPSC induced forebrain cells, they were collected from CTR organoids, CHOL organoids, and semaglutide-treated CHOL+SEMA organoids at day 30. Two biological replicates were included in each group. Organoids were pooled respectively and washed three times with pre-cold PBS. Single-cell suspensions were prepared by incubating with 0.5 mg/mL digestive enzymes 1 for 30 min at 37 °C in a water bath. After, suspensions were filtered through a 70 μM cell strainer (BD Falcon, 352350). After centrifugation at 500 g for 5 min, the cell precipitated was resuspension with PBS+0.01%BSA.

The MGI DNBelab C-TaiM4 platform utilizes microfluidic technology to encapsulate single cells with mRNA capture magnetic beads containing unique cell barcodes (Cell Barcodes) and unique molecular identifiers (UMIs) within oil droplets. The platform employs a dual-magnetic bead system (mRNA capture beads and droplet-identification beads) to enhance capture efficiency and accuracy. Then, cell lysis was completed in the droplet, and mRNA molecules were captured by Oligo (dT) on the magnetic beads and reverse transcribed to generate cDNA with cell barcodes and UMIs.

For library construction, the cDNA was purified, amplified, and ligated with sequencing adapters to generate the final sequencing library. Library quality was checked using an Agilent 2100 Bioanalyzer (Agilent Technologies, USA). Finally, qualified libraries were sequenced in PE100 mode using DNBSEQ-T7 from BGI. The cDNA library sequencing depth was approximately 450M Reads/library, and the Oligo library sequencing depth was approximately 50M Reads/library. scRNA-seq were performed by Hangzhou Astrocyte Technology Co,.Ltd.

scRNA-seq Data Pre-processing and Quality Control

Using the official BGI software DNBC4Tools with parameter settings, we performed filtering, alignment, quantification, and cell identification/recovery of raw data. After transcriptomic normalization processing, gene expression matrix files for each cell were obtained. The resulting gene expression matrices were imported into R (v.4.4.1) and processed using the Seurat package (v.5.3.1) for integration and quality control. rigorous filtering criteria were applied to retain high-quality cells: (1) 200 < total detected genes < 12,500; (2) total unique molecular identifier (UMI) counts > 500; (3) log10(GenesPerUMI) > 0.8; and (4) mitochondrial mRNA content < 20% and ribosomal mRNA content < 30%.

Data analysis: Colocalization ratio of images

Confocal images were initially processed by selecting regions of interest (ROIs) and applying adaptive thresholding for binarization. Different adaptive threshold methods were used for various antibodies. The binarized images were then batch-processed using the ‘Colocalization

Finder' plugin in Fiji. A script for processing colocalization in Fiji, along with detailed methods, is available at the provided GitHub link.

Data analysis: Excitatory synapse and inhibitory synapse

The images underwent preliminary processing, which involved selecting regions of interest (ROIs) and applying adaptive thresholding techniques. Synapse numbers were quantified using the 'Puncta Analyzer' plugin in Fiji.

Calcium imaging and analysis

Brain organoids were cultured using the microwell air-liquid interface attachment method 43. Perform two medium changes using BrainPhys™ Neuronal Medium before beginning incubation with Flou-4 calcium indicator (Invitrogen, Catalog # F14201). Using the complete culture medium, prepare a 5 μM Flou-4 solution, add 200 μL to a single well and incubate for 2 hours in the incubator. Make two medium changes and add 500 μL of BrainPhys™ Neuronal Medium (STEMCELL Technologies, Catalog # 05790) 30 minutes prior to baseline imaging. Baseline imaging was performed using a confocal microscope (NikonA1R) for 5 minutes with no delay between frames, and the frame rate was 7.67. After baseline imaging, neurotransmitter drugs, GABA (Sigma-Aldrich, Catalog # 56-12-2) 100 μM, were added for final concentration. After 1 minute incubation, change the medium twice and add 200 μL BrainPhys™ Neuronal Medium. Immediately image, keeping the field of view and parameters the same as the baseline image.

For batch processing in calcium imaging data analysis, CNMF-E44 was used. The code for parameters (getmat.m) can be found in the source. The sum of neuron.S, representing all neurons in the view, is recorded as the total number of spikes after processing. The number of active cells is recorded as the number of rows of neuron.S, i.e. the ROI where the spike is detected. The calcium trace overlay plot is presented by CNMFeClustering[29]. Calcium imaging analysis of microglia was initially conducted by isolating each microglial cell based on the maximum intensity projection of image sequences in the Cell Tracker channel. Subsequently, the Fluo-4 AM sequence image data for each isolated microglia was analyzed. Spikes were defined and quantified using a specific code, which is provided for reference.

Statistical analysis

All statistical analyses in this study were conducted using commercially available software, namely Prism and Excel. Data from replicates are presented as mean ± standard error of the mean (SEM). The methodology for analyzing differences between multiple groups is detailed in the figure legends accompanying each graph. For the creation of graphical representations, Adobe Illustrator 2024 and Biorender were utilized.

Data availability

Raw images of the cytokine arrays have been made available in the source data, which can be accessed via the provided Github link: *https://github.com/FengYilinElaine/2-3D-AD-oranoids*. Bulk RNA-seq data have been deposited at GEO and are publicly available as of the date of publication. Microscopy data reported in this paper will be shared by the lead contact upon request.

Acknowledgements

The work was supported by the National Key Research and Development Program of China (2024YFA0919800); Shenzhen Medical Academy of Research and Translation, SMART, B2402009; National natural science foundation of China (32371470); Key-Area Research and Development Program of Guangdong (2023B0909020003), and Shenzhen Natural Science Foundation (QNXMA20250701093300001, JCYJ20241202123909013).

Additional information

Author contributions

S.M. conceived and supervised the work. Y.F. wrote the manuscript and generated the figures. Y.F., F.Y., H.Z. and J.T. performed the experiments. Y.F., H.Z., J.T., P.E.L. and S.M. edited the final manuscript.

Funding

Funder	Grant reference number	Author
MOST | National Key Research and Development Program of China (NKPs)	2024YFA0919800	Shaohua Ma
Shenzhen Medical Academy of Research and Translation	B2402009	Shaohua Ma

Author ORCID iDs

Shaohua Ma: https://orcid.org/0000-0002-4995-2032

References

1. **Iwatsubo T,** et al. (1994) Visualization of Aβ42(43) and Aβ40 in senile plaques with end-specific Aβ monoclonals: Evidence that an initially deposited species is Aβ42(43). *Neuron* **13**:45-53 https://doi.org/10.1016/0896-6273(94)90458-8 | PubMed
2. **Hampel H,** et al. (2021) The Amyloid-β Pathway in Alzheimer's Disease. *Molecular Psychiatry* **26**:5481-5503 https://doi.org/10.1038/s41380-021-01249-0 | PubMed
3. **Michell-Robinson MA,** et al. (2015) Roles of microglia in brain development, tissue maintenance and repair. *Brain* **138**:1138-1159 https://doi.org/10.1093/brain/awv066 | PubMed
4. **Chen Y,** Colonna M (2022) Two-faced behavior of microglia in Alzheimer's disease. *Nature Neuroscience* **25**:3-4 https://doi.org/10.1038/s41593-021-00963-w | PubMed
5. **Habib N,** et al. (2020) Disease-associated astrocytes in Alzheimer's disease and aging. *Nature Neuroscience* **23**:701-706 https://doi.org/10.1038/s41593-020-0624-8 | PubMed
6. **Heneka MT,** et al. (2015) Neuroinflammation in Alzheimer's disease. *Lancet Neurol* **14**:388-405 https://doi.org/10.1016/s1474-4422(15)70016-5 | PubMed
7. **Patani R,** Hardingham GE, Liddelow SA (2023) Functional roles of reactive astrocytes in neuroinflammation and neurodegeneration. *Nature Reviews Neurology* 1-15 https://doi.org/10.1038/s41582-023-00822-1 | PubMed
8. **Hobson R,** et al. (2026) Clonal CD8+ T cels populate the leptomeninges and coordinate with immune cells in human degenerative brain diseases. *Nature* **27**:323-335 https://doi.org/10.1038/s41590-025-02401-6 | PubMed
9. **Feng Y,** et al. (2023) Stress regulates Alzheimer's disease progression via selective enrichment of CD8+ T cells. *Cell Reports* **42**:113313 https://doi.org/10.1016/j.celrep.2023.113313 | PubMed
10. **Ma W,** et al. (2023) The intricate role of CCL5/CCR5 axis in Alzheimer disease. *Journal of Neuropathology & Experimental Neurology* **82**:894-900 https://doi.org/10.1093/jnen/nlad071 | PubMed
11. **Festa BP,** et al. (2023) Microglial-to-neuronal CCR5 signaling regulates autophagy in neurodegeneration. *Neuron* https://doi.org/10.1016/j.neuron.2023.04.006 | PubMed
12. **Shi Z,** et al. (2023) Microglia drive transient insult-induced brain injury by chemotactic recruitment of CD8(+) T lymphocytes. *Neuron* **111**:696-710.e699, https://doi.org/10.1016/j.neuron.2022.12.009 | PubMed

13. **Su W,** et al. (2023) CXCR6 orchestrates brain CD8+ T cell residency and limits mouse Alzheimer's disease pathology. *Nature Immunology* **24**:1735-1747 https://doi.org/10.1038/s41590-023-01604-z | PubMed

14. **Feng Y,** et al. (2023) Protocol for generating in vitro glioma models using human-induced pluripotent- or embryonic-stem-cell-derived cerebral organoids. *STAR Protoc* **4**:102346 https://doi.org/10.1016/j.xpro.2023.102346 | PubMed

15. **Zheng H,** et al. (2025) Astrocyte-secreted cues promote neural maturation and augment acitivity in human forebrain organoids. *Nature Communication* **16**:2845 https://doi.org/10.1038/s41467-025-58295-3 | PubMed

16. **Pasca SP,** et al. (2025) A framework for neural organoids, assembloids and transplantation studies. *Nature* **639**:315-320 https://doi.org/10.1038/s41586-024-08487-6 | PubMed

17. **Park DS,** et al. (2023) iPSC-cell-derived microglia promote brain organoid maturation via cholesterol transfer. *Nature* **623**:397-405 https://doi.org/10.1038/s41586-023-06713-1 | PubMed

Peer reviews

Reviewer #1 (Public review):

Summary:

A growing body of evidence indicates that Alzheimer's disease is not simply a disease of neurons accumulating toxic protein aggregates, but one in which the immune system, both its resident brain component and its circulating peripheral arm, plays an active and sustained role. Understanding how these two immune compartments interact with one another and with diseased neural tissue has been hampered by the fact that the mouse immune system differs fundamentally from the human one in ways likely to matter for disease progression. The authors set out to address this gap by building a modular laboratory model that brings together three human cell types in a three-dimensional setting: brain organoids derived from human stem cells to provide a neural substrate, stem cell-derived brain immune cells (microglia) to represent the resident immune compartment, and circulating immune cells (CD8-positive T cells) harvested from human blood to represent the peripheral adaptive immune response. By exposing this tri-cellular system to a toxic form of amyloid protein, the hallmark aggregating molecule of Alzheimer's disease, the authors aimed to dissect, step by step, how microglia respond to amyloid stress, what inflammatory signals they release as a consequence, and whether those signals are sufficient to attract T cells into the neural environment. They further aimed to test whether blocking the molecular receptors that guide T cell movement could interrupt this process, with the broader goal of positioning the platform as a tool for human-relevant drug screening.

Strengths

The conceptual architecture of the platform is one of its clearest strengths. The decision to add immune components in a stepwise, modular fashion, first characterising the neural response to amyloid, then adding microglia, then adding T cells, makes it possible to attribute observed changes to specific cellular contributions in a way that a more complex all-at-once model would not allow. This staged design is well thought-through, and its logic is clearly communicated. The combination of single-cell transcriptional profiling, calcium imaging for real-time functional readouts, transwell migration assays, and protein secretion measurements gives the study a genuinely multi-modal character that goes beyond what purely transcriptomic or purely imaging-based approaches can offer. The observation that T cells failed to migrate toward amyloid-treated organoids in the absence of microglia is a clean and conceptually important result, clearly supporting the idea that the resident immune response acts as an intermediary between amyloid pathology and the recruitment of peripheral immune cells. The identification of specific chemokine receptor pathways

mediating T cell movement and the demonstration that pharmacological blockade of those receptors reduces migration and provide a degree of mechanistic resolution useful for thinking about future therapeutic strategies.

Weaknesses

Despite these strengths, several aspects of the work as presented substantially limit the confidence one can place in its conclusions.

The most consequential issue concerns the origin of the cells used in the model. The three cellular components: the brain organoids, the microglia, and the T cells are derived from genetically unrelated individuals. The T cells, in particular, come from healthy blood donors unrelated to the stem cell lines used to generate the neural tissue. This means the immune cells and the tissue they are interacting with carry different molecular identity markers (the proteins that the immune system uses to distinguish self from non-self). In this setting, any T cell activation or directed movement could reflect a generic rejection-like response to foreign tissue rather than a disease-relevant, chemokine-directed recruitment process. This is not a subtle concern: it represents a fundamental ambiguity at the heart of the model's central finding, and it is not acknowledged anywhere in the manuscript. For the transwell migration data to be interpretable as a model of Alzheimer's disease rather than of immune incompatibility, the authors would need to demonstrate that migration is driven by the specific chemokine environment and not by the genetic mismatch between cells, for example, using cells from the same donor or from matched donors, or by showing that blocking identity-marker recognition does not alter migration.

A related concern is that the T cells used are from healthy individuals, whereas T cells from people with Alzheimer's disease are known to differ in their activation state, surface receptor expression, and functional behaviour. The platform cannot yet claim to model the specific T cell biology of Alzheimer's disease until disease-relevant T cells are incorporated.

Beyond this foundational issue, the study frequently describes findings in causal terms that the experimental design does not support. The resident immune cells are said to "drive" T cell recruitment and "establish" a feedback loop. These are strong mechanistic claims. The evidence presented indicates that when microglia are present, more T cells migrate, and that blocking T cells receptors reduces migration. What is missing is direct evidence that the specific molecules measured, particularly the chemokines CCL4 and CCL5, are the agents responsible, as opposed to other signals also present in the conditioned environment. No experiment directly neutralises these chemokines to test whether their removal is sufficient to abolish T cell recruitment. Without such an experiment, the receptor-blocking data show only that the receptors matter, not that the measured ligands are the ones activating those receptors.

The abstract describes one particular molecule, CXCL10, as a contributor to T cell recruitment, but the data in the paper itself show no significant change in CXCL10 levels between conditions. This discrepancy between the abstract and the results is misleading to readers who may not read the figures in detail.

The single-cell sequencing data, which form the basis for claims about changes in cell populations following amyloid treatment or microglia addition, are presented without validation of the cell type labels against established reference datasets from human brain tissue. The proportional shifts in cell populations between conditions (Figures 1H and 3E) are described as significant findings but are shown without any statistical test appropriate for this type of compositional data. Comparisons of cell-type proportions derived from single-cell sequencing require specialised statistical approaches that account for the interdependence of proportions and the variability between samples; standard tests are not appropriate here, and none are applied.

There is also an unresolved inconsistency in the age at which the organoids were analysed by single-cell sequencing: the text states day 90, while the figure legend states day 60, and the methods section contains a passage describing experimental conditions (including a cholesterol treatment and a drug called semaglutide) that are entirely unrelated to this study and appear to have been copied from a different manuscript. These issues raise concerns about the rigour of the manuscript preparation and should be corrected.

Finally, the sample sizes underpinning several key conclusions are small (typically three to four organoids per group), particularly for the protein-secretion measurements used to identify the inflammatory signals responsible for T cell recruitment. While organoid studies are inherently limited in scale, the strength of the mechanistic claims made here would benefit from larger sample size or independent experimental replication.

Conclusion:

The authors have built a platform that is conceptually well-conceived and generates data consistent with a role for microglia in bridging amyloid pathology and T cell recruitment. In that sense, they have made meaningful progress toward their stated aims. However, the platform, as described, cannot yet deliver the human-specific mechanistic insight it claims to provide, primarily because the non-autologous configuration of the model introduces an uncontrolled variable that confounds the interpretation of the immune interaction data. The claim to have provided "the first human-specific mechanistic demonstration" of microglial activation as a bridge between amyloid pathology and adaptive immune recruitment is not supported by the evidence presented. The data are consistent with this interpretation but do not establish it.

The general approach, building increasingly complex human neural-immune models by adding components in a controlled, stepwise manner, is a valuable direction for the field and one that other groups working on neuroinflammation will find useful to consider. The combination of live calcium imaging and transcriptional profiling in the same experimental system is a practical contribution that demonstrates the kind of multi-modal readout this class of model can support. If the autologous confound is resolved in future iterations and if the mechanistic claims are grounded in more direct experimental evidence, this type of platform could become a genuinely useful tool for investigating human neuroimmune biology and for screening candidate therapeutic compounds in a human-relevant context. As currently presented, however, readers and researchers considering adopting this approach should be aware that the immune interaction data may reflect genetic mismatches between cell sources rather than disease-specific biology, and that the causal conclusions drawn from the chemokine and migration data go beyond what the experiments can support.

https://doi.org/10.7554/eLife.111730.1.sa1

Reviewer #2 (Public review):

Summary:

In this study, the authors developed a human forebrain organoid model incorporating both iPSC-derived microglia and $CD8^+$ T cells, enabling them to recreate and investigate multicellular aspects of AD pathology in a human-relevant system.

Their findings show that microglia help clear amyloid-β deposits, but they also promote inflammatory responses. Activated microglia recruit $CD8^+$ T cells by releasing the chemokines CCL4, CCL5, and CXCL10, which signal through the receptors CCR1/CCR5 and CXCR3. Pharmacological inhibition of CCR5 or CXCR3 prevents T-cell recruitment and alters autophagy pathways in a microglia-dependent manner.

Strengths:

The study presents a versatile human organoid platform for investigating neuron-immune interactions in Alzheimer's disease. It highlights the critical role of microglia-driven recruitment of $CD8^+$ T cells in sustaining neuroinflammation and identifies CCR5 and CXCR3 signaling pathways as promising therapeutic targets for neuroinflammatory conditions.

This study is interesting and presents novel findings supported by state-of-the-art approaches, including single-cell RNA sequencing, a three-dimensional cerebral organoid model, and co-culture systems involving two distinct immune cell populations.

Weaknesses:

Several aspects of the study require clarification and further improvement. For example:

(1) Figure 1H is missing statistical analyses.

(2) The scRNA-seq analysis shows a reduction in the proportion of cells occupying transcriptional states associated with later pseudotime values, which the authors interpret as evidence that Aβ treatment inhibits neuronal maturation. However, the data presented do not appear sufficient to support this conclusion. An alternative explanation is that Aβ preferentially affects the survival of more mature neuronal populations, leading to their depletion, consequently, an apparent enrichment of cells at earlier pseudotime states. Therefore, the observed pseudotime shift does not necessarily demonstrate impaired maturation per se. The authors should revise the interpretation of these results in the first paragraph and either provide additional evidence supporting a maturation defect or discuss alternative explanations such as selective loss of mature neurons.

(3) A similar concern applies to the scRNA-seq data presented in Figure 3. The authors interpret the shift toward later pseudotime states in the presence of microglia as evidence of enhanced neuronal maturation. However, the data do not exclude alternative explanations. For instance, microglia may preferentially promote the survival of more mature neuronal populations or protect them from cell death, thereby increasing their relative abundance in the dataset. Consequently, the observed pseudotime distribution cannot be taken as direct evidence of enhanced maturation. The authors should revise their interpretation accordingly and discuss the possibility that the observed effect reflects differential survival rather than accelerated neuronal maturation.

(4) In Figures 4A-E, the authors should report the levels of the secreted proteins in pg/mL instead of relative values, as this would better reflect the actual amounts produced. In Figure 4H, the inhibitor-treated control T-cell samples should be included. Furthermore, it should be explicitly stated that the inhibitor-treated data points currently shown refer to T cells cultured in the presence of myeloid Aβ.

https://doi.org/10.7554/eLife.111730.1.sa0